Crystal Structure of Formate Dehydrogenase H: Catalysis Involving Mo, Molybdopterin, Selenocysteine, and an Fe_4S_4 Cluster

Jeffrey C. Boyington, Vadim N. Gladyshev,*
Sergei V. Khangulov, Thressa C. Stadtman, Peter D. Sun†

Formate dehydrogenase H from *Escherichia coli* contains selenocysteine (SeCys), molybdenum, two molybdopterin guanine dinucleotide (MGD) cofactors, and an Fe_4S_4 cluster at the active site and catalyzes the two-electron oxidation of formate to carbon dioxide. The crystal structures of the oxidized [Mo(VI), $Fe_4S_{4(ox)}$] form of formate dehydrogenase H (with and without bound inhibitor) and the reduced [Mo(IV), $Fe_4S_{4(red)}$] form have been determined, revealing a four-domain αβ structure with the molybdenum directly coordinated to selenium and both MGD cofactors. These structures suggest a reaction mechanism that directly involves $SeCys^{140}$ and His^{141} in proton abstraction and the molybdenum, molybdopterin, Lys^{44}, and the Fe_4S_4 cluster in electron transfer.

Formate dehydrogenase H (FDH_H), a 79-kD polypeptide that oxidizes formate to carbon dioxide with the release of a proton and two electrons, is a component of the anaerobic formate hydrogen lyase complex of *E. coli* (*1*). Essential to its catalytic activity are an Fe_4S_4 cluster, a Mo atom that is coordinated by two MGD cofactors, and a SeCys residue (*2*–*4*). With the recent determination of the crystal structures of three other molybdopterin (MPT)–containing enzymes (*5*–*8*), a functional role for the Mo-MPT cofactor has begun to emerge. However, the precise role of the active site selenium in this type of selenoenzyme and its interaction with Mo-MPT cofactors and the Fe_4S_4 cluster remains to be elucidated (*9*).

The structure of *E. coli* FDH_H, as solved by multiple isomorphous replacement (MIR) and multiwavelength anomalous dispersion (MAD) methods (Table 1), consists of four αβ domains (Fig. 1). The first domain (residues 1 to 60, 448 to 476, and 499 to 540), comprising two small antiparallel β sheets and four helices, coordinates the Fe_4S_4 cluster just below the protein surface. The MGD-binding domains II (residues 61 to 135, 336 to 447, and 477 to 498) and III (residues 136 to 335) are each αβα sandwiches with overall topologies that closely resemble the classical dinucleotide-binding fold (*10*). A marked twofold pseudosymmetry is observed relating the central portions of domains II and III. Despite their low sequence homology (<20% identity), the two domains can be superimposed to a root-mean-square (rms) deviation of 1.2 Å for 56 α carbons. $SeCys^{140}$, an essential ligand to Mo, is located in a short loop at the NH_2-terminus of domain III. The COOH-terminal domain (residues 541 to 715) consists of a six-stranded mixed β barrel and five helices.

Similar to the active sites observed in aldehyde ferredoxin oxidoreductase and dimethyl sulfoxide (DMSO) reductase, the active site Mo of FDH_H is coordinated by two tightly bound MGD cofactors, each containing a tricyclic ring system with a pyran ring fused to the pterin (*6*, *7*). The Mo di(MGD) of FDH_H is ligated within the interfaces of all four domains through an extensive network of hydrogen bonds, salt bridges, and van der Waals interactions, most of which involve domains II, III, and IV (Fig. 2). Domain II exclusively coordinates MGD^{801} while domain III coordinates MGD^{802}. Domain IV forms a cap over the bound pterin cofactors as it straddles domains II and III. Of the 35 residues that coordinate the Mo di(MGD) cofactor through hydrogen bonds, 23 are well conserved among the known MGD-containing formate dehydrogenases (*11*); the remaining 12 residues interact primarily through main chain hydrogen bonds (Fig. 2).

In both the reduced Mo(IV) and oxidized Mo(VI) structures, Mo is ligated to the four *cis*-dithiolene sulfurs of the MGD cofactors and the selenium of $SeCys^{140}$. The coordination geometry of Mo in formate-reduced FDH_H is closely approximated by a square

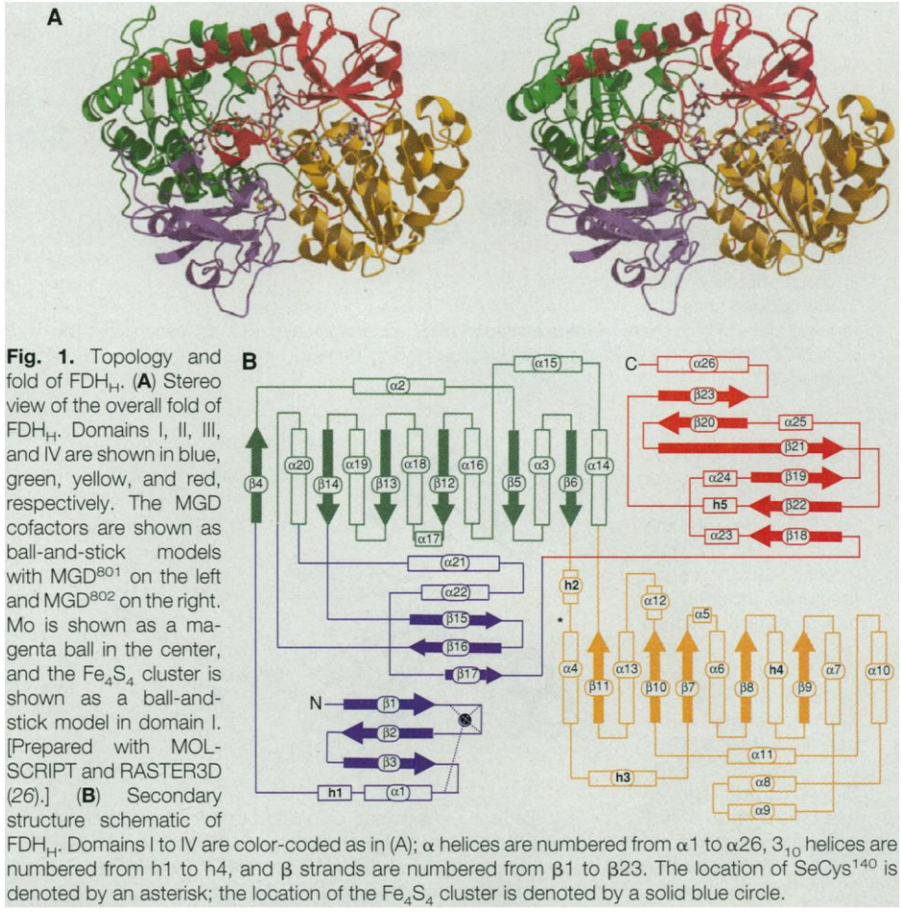

Fig. 1. Topology and fold of FDH_H. (**A**) Stereo view of the overall fold of FDH_H. Domains I, II, III, and IV are shown in blue, green, yellow, and red, respectively. The MGD cofactors are shown as ball-and-stick models with MGD^{801} on the left and MGD^{802} on the right. Mo is shown as a magenta ball in the center, and the Fe_4S_4 cluster is shown as a ball-and-stick model in domain I. [Prepared with MOLSCRIPT and RASTER3D (*26*).] (**B**) Secondary structure schematic of FDH_H. Domains I to IV are color-coded as in (A); α helices are numbered from α1 to α26, 3_{10} helices are numbered from h1 to h4, and β strands are numbered from β1 to β23. The location of $SeCys^{140}$ is denoted by an asterisk; the location of the Fe_4S_4 cluster is denoted by a solid blue circle.

J. C. Boyington and P. D. Sun, Structural Biology Section, Laboratory of Molecular Structure, National Institute of Allergy and Infectious Diseases, National Institutes of Health (NIH), 12441 Parklawn Drive, Rockville, MD 20852, USA.
V. N. Gladyshev and T. C. Stadtman, Laboratory of Biochemistry, National Heart, Lung, and Blood Institute, NIH, 9000 Rockville Pike, Bethesda, MD 20892, USA.
S. V. Khangulov, Department of Chemistry, Hoyt Laboratory, Princeton University, Princeton, NJ 08544, USA.

*Present address: Basic Research Laboratory, National Cancer Institute, NIH, 9000 Rockville Pike, Bethesda, MD 20892, USA.
†To whom correspondence should be addressed.

pyramid in which the sulfur atoms provide the four equatorial ligands and the selenium provides an axial ligand (Fig. 3) (*12*). The Mo atom is ~0.4 Å above the equatorial plane in the direction of the selenium. Upon oxidation of Mo(IV) to Mo(VI), however, the pterin portion of MGD[801] is rotated 27° away from the equatorial plane and 16° along its own long axis. In contrast, little movement is observed in MGD[802] or in the guanine nucleotide portion of MGD[801]. The fifth ligand, the selenium atom of SeCys[140], moves 0.9 Å closer to S12 of MGD[802], resulting in a slightly longer bond to Mo (2.7 Å). The four sulfur ligand distances to Mo also increase slightly (to between 2.3 and 2.6 Å) in the oxidized state (*12*). $F_{obs} - F_{calc}$ electron density maps revealed the presence of a sixth ligand in the Mo(VI) state, giving the Mo a trigonal prismatic coordination geometry (Fig. 3). This ligand was modeled as a hydroxyl group that refined to a distance of 2.2 Å from Mo with a *B* factor of 16.8 Å^2. The position of the SeCys[140] β carbon in the oxidized state also enables a new water molecule, H_2O^{64}, to interact with the amide of His[141] and the NH1 of Arg[333], whose side chain moves 3.9 Å toward H_2O^{64}. Redox-induced conformational changes result in minor domain movements and minor alterations in the hydrogen-bonding network coordinating MGD[801] (Fig. 2).

The binding of the nitrite inhibitor (*2*, *3*) to the oxidized FDH_H is clearly visible in the initial $F_{obs} - F_{calc}$ electron density map as a crescent-shaped 4σ peak indicating displacement of the hydroxyl ligand originally at the same position (Fig. 4). One nitrite oxygen is bound to the Mo (bond length 2.5 Å); the other is hydrogen-bonded to both the main chain amide of His[141] and the side chain of Arg[333], which moves 0.5 Å closer to Mo in order to accommodate this hydrogen bond. Nitrite also displaces the H_2O^{64} observed in oxidized FDH_H. Both Arg[333] and His[141] are strictly conserved in all Mo-dependent formate dehydrogenases (*11*). Apart from the nitrite-binding site, the structure of inhibitor-complexed oxidized FDH_H is essentially the same as that of the benzyl viologen–oxidized enzyme. When formate is modeled into the nitrite-binding site, the α proton of formate is located less than 1.5 Å from the selenium of SeCys[140], poising it for abstraction by selenium. The side chain of His[141] is positioned on the other side of the selenium, opposite the formate. This putative substrate-binding site lies at the bottom of a deep crevice located between domains II and III, with Arg[333] at the base of the crevice providing both a positive charge and a critical hydrogen bond for orienting the substrate for catalysis.

Kinetic experiments have suggested that the two electrons from oxidized formate leave the enzyme one at a time through a ping-pong mechanism (*3*). The Fe_4S_4 cluster located just below the protein surface in domain I provides a one-electron sink for a downstream electron acceptor. The observed reduction of the Fe_4S_4 cluster upon substrate binding indicates that electrons must travel from the Mo center to the Fe_4S_4 cluster. The most direct path between the Mo atom and the Fe_4S_4 cluster is through the partially conjugated ring system of MGD[802], exiting through N20 and following the hydrogen bond pathway from H_2O^{30} to the Nζ of Lys[44] to the S1 of the Fe_4S_4 cluster (Fig. 5). Both H_2O^{30} and the Nζ of Lys[44] have well-ordered electron densities with temperature factors in the reduced form of 21.7 and 27.9 Å^2, respectively. Lys[44], although strictly conserved in the family of MGD-containing formate dehydrogenases (*11*), is completely buried in the interior of the protein and has no countercharge partner with which to interact.

Catalysis begins with formate replacing the Mo-bound hydroxyl in the [Mo(VI), $Fe_4S_{4(ox)}$] state of the enzyme, presumably

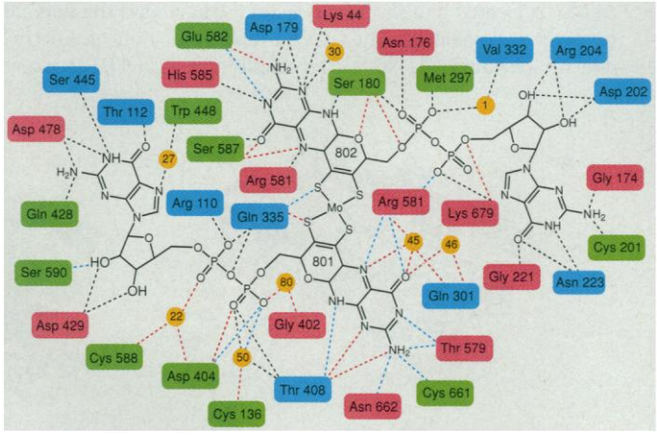

Fig. 2. Schematic representation of the hydrogen-bonding network coordinating MGD[801] and MGD[802]. Residues are color-coded according to sequence conservation among the known sequences of MGD-containing FDH enzymes (*11*): magenta, invariant; blue, well conserved; and green, not conserved. The eight water molecules involved in hydrogen-bonding interactions are designated by orange circles. Hydrogen bonds present in the oxidized state, the reduced state, or both states are represented by blue, red, or black dashed lines, respectively. The binding of both MGD cofactors resembles the dinucleotide binding observed in the classical dinucleotide-binding proteins (*10*).

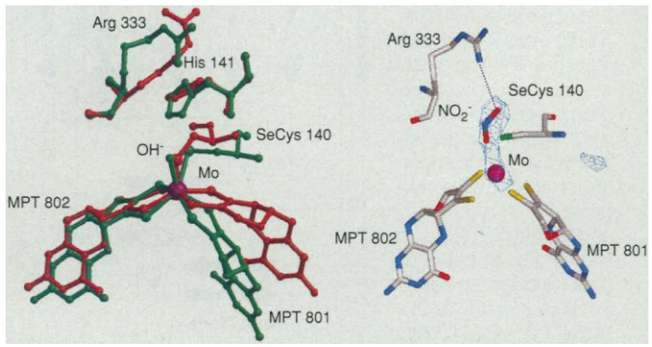

Fig. 3 (left). Superposition of the Mo center of FDH_H in the reduced [Mo(IV)] state (red) and oxidized [Mo(VI)] state (green). The Mo center (magenta) includes the active site residues SeCys[140], His[141], and Arg[333] and the pterin portions (MPT) of the Mo cofactors. [Prepared with MOLSCRIPT and RASTER3D (*26*).]

Fig. 4 (right). The nitrite-binding site. A 4σ $F_{obs} - F_{calc}$ electron density map calculated to 2.9 Å using phases from the uncomplexed oxidized FDH_H reveals the binding of the inhibitor nitrite. [Prepared with SETOR (*27*).] The coordinates for the reduced, oxidized, and nitrite-bound forms of FDH_H have been deposited in the Protein Data Bank (accession numbers 1aa6, 1fdo, and 1fdi, respectively).

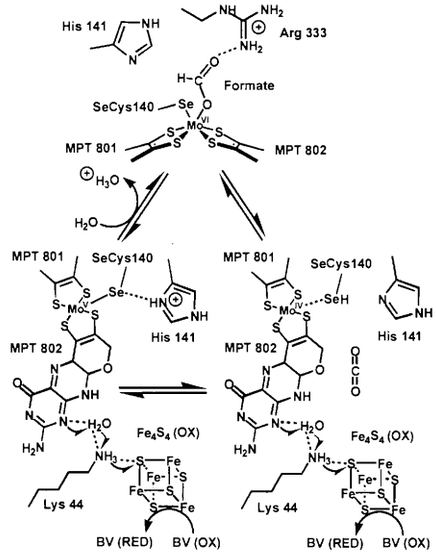

Fig. 5. The proposed reaction mechanism for FDH_H. BV, benzyl viologen.

being stabilized and oriented by hydrogen bonding through a carbonyl oxygen of formate to both Arg^{333} and the amide nitrogen of His^{141} (Fig. 5). The subsequent oxidation of formate to carbon dioxide and the transfer of two electrons to the Mo center (Fig. 5) may occur either by a direct two-electron transfer through the oxygen of formate to Mo or by a direct hydride transfer to Mo. Upon Mo reduction, the α proton of formate is released to the nearby His^{141} through protonation of $SeCys^{140}$. The involvement of a histidine residue is consistent with known pH dependencies in the catalytic activity of both the $SeCys^{140} \rightarrow Cys^{140}$ mutant and wild-type FDH_H (*13*), and the protonation of His^{141} by the α proton of formate is supported by electron paramagnetic resonance (EPR) observations (*14*). The next step is to shuttle electrons from the Mo(IV) to a downstream electron acceptor through the Fe_4S_4 cluster. As the first electron is transferred through Lys^{44} to the Fe_4S_4 cluster, it produces an intermediate [Mo(V), $Fe_4S_{4(red)}$] that is easily observed in EPR experiments (*14*). Meanwhile, the transfer of a formate-derived proton to His^{141} will lead to hydrogen bond formation between the imidazole of His^{141} and the selenium of $SeCys^{140}$ while the selenium is coordinated to Mo(V) (*15*). Although the nature of the in vivo electron acceptor for FDH_H remains unknown, the reoxidation of the Fe_4S_4 can be achieved with benzyl viologen, a one-electron acceptor. Once the Fe_4S_4 cluster is reoxidized, a second electron can be transferred from Mo(V) to the Fe_4S_4 cluster and the enzyme returns to its initial state after the second oxidation of the Fe_4S_4 cluster. The oxidation of Mo(V) to Mo(VI) would cause the hydrogen bond between $SeCys^{140}$ and His^{141} to break, thereby releasing the proton of His^{141} to solvent.

A common feature among many MPT-containing enzymes is the coupling of the redox state of Mo with the substrate oxidation-reduction process. In FDH_H, the reduction of Mo(VI) to Mo(IV) profoundly affects the Mo coordination geometry and thus the conformation of MPTs. Such changes, which are also observed in model compounds (*16*), may represent a general feature associated with MPT-dependent Mo- and W-containing enzymes. In contrast, the incorporation of a SeCys in FDH_H, as compared with incorporation of a Cys or Ser in other di(MPT)-dependent enzymes, appears to correlate with the usage of a hydroxyl ligand as opposed to sulfido or oxo ligands to Mo (*7, 17, 18*). This is also evident in extended x-ray absorption fine structure (EXAFS) studies of FDH_H where a terminal oxo ligand to Mo is observed in a $SeCys^{140} \rightarrow Cys^{140}$ mutant but not in wild-type FDH_H (*19*). This mutation results in a much lower initial rate of substrate oxidation, 1/300 that of the wild type (*13*). Thus, the choice of a SeCys, Cys, or Ser ligand to Mo may serve to fine-tune the coordination of a particular cis-ligand and hence set the substrate preference. This suggests a new role of selenium in biology, involving ligation to a metal and proton transfer during catalysis.

The combination of the MPT redox center, $SeCys^{140}$, and the Fe_4S_4 cluster, each precisely positioned, results in an enzyme that not only catalyzes the oxidation of formate but also effectively couples the oxidoreduction to an electron acceptor in the formate hydrogen lyase complex. This suggests that the MPT moiety, in addition to providing a structural framework for Mo coordination, also functions as part of an electron transfer path and potentially as an electron sink.

Table 1. Data collection, phasing, and refinement statistics for FDH_H structure determination. Purification, crystallization, and cryofreezing of reduced FDH_H crystals [Mo(IV), $Fe_4S_{4(red)}$] were performed in a nitrogen atmosphere at <1 ppm of oxygen as described (*20*). Crystals belong to the tetragonal space group $P4_12_12$ with cell dimensions of $a = b = 146.3$ Å and $c = 82.3$ Å containing one monomer in the asymmetric unit. Crystals of FDH_H in the [Mo(VI), $Fe_4S_{4(ox)}$] state (*10*) were obtained by serially washing crystals in a formate-free solution and then soaking crystals in 10 mM benzyl viologen for 30 min before freezing. Crystals of nitrite-inhibited FDH_H were obtained by adding 30 mM sodium nitrite to the benzyl viologen solution during oxidation. Diffraction data were processed with DENZO and SCALEPACK (*21*) or R-AXIS software (*22*) and scaled with CCP4 programs (*23*). MIR phases from five derivatives [K_2PtCl_4, $Sm(OAc)_3$, AuCN, TMLA, and $Pb(OAc)_2$] together with MAD and anomalous scattering phases (AuCN and TMLA derivatives, respectively) were refined using MLPHARE (*23*), combined with SIGMAA (*23*) and subsequently improved through solvent flattening and histogram matching using the program DM (*23*). The resulting electron density maps were readily interpretable. Model building and refinement were carried out with the programs O (*24*) and X-PLOR 3.1 (*25*). The refinement process used all data for which $|F| > 2\sigma_F$. Values of I/σ_I for the reduced, oxidized, and NO_2^--bound data sets were 26.1, 22.1, and 19.5, respectively. During the refinement, ligand bonds to Mo were only loosely restrained (1.0 kcal/Å) and the position of the selenium in reduced FDH_H was fixed.

Data set*	Wavelength (Å)	d_{min} (Å)	Reflections		Completeness (%)	R_{sym}§	Sites (*N*)	Phasing power‖
			Measured	Unique				
Native 1	1.5418†	3.0	194,324	17,511	96.0	8.8	–	–
K_2PtCl_4	1.5418†	3.0	188,492	18,059	97.5	11.2	3	0.71
$Sm(OAc)_3$	1.5418†	3.0	160,269	16,644	90.3	10.5	2	0.45
AuCN	1.5418†	3.0	161,232	18,353	99.6	10.1	6	0.95
TMLA	1.5418†	3.5	142,691	11,327	95.9	6.1	7	1.29
$Pb(OAc)_2$	1.5418†	3.0	183,543	18,514	99.6	8.2	3	0.72
Oxidized	1.5418†	2.8	84,166	20,861	93.4	7.9	–	–
NO_2^-	1.5418†	2.9	94,068	19,946	97.7	9.0	–	–
Native 2	1.0402‡	2.3	169,244	36,025	88.0	8.5	–	–
AuCNλ1	1.0489‡	3.0	59,714	26,227	75.3	4.3	–	–
AuCNλ2	1.0402‡	3.0	59,419	26,306	75.4	4.3	8	0.64
AuCNλ3	1.0398‡	3.0	51,813	25,231	72.4	4.3	8	0.46
TMLAλ2	0.9493‡	3.0	88,083	29,933	85.7	4.0	8	1.28

FDH model	*d* spacings (Å)	*R* value	R_{free}	Non-H atoms (*N*)	Solvent sites (*N*)	Mean *B* factor (Å²)	rmsd	
							Bonds (Å)	Angles (°)
Reduced	6.0 to 2.3	0.217	0.287	5541	83	28.4	0.013	1.81
Oxidized	6.0 to 2.8	0.195	0.288	5668	64	24.1	0.012	1.81
NO_2^--bound	6.0 to 2.9	0.192	0.282	5671	62	24.1	0.012	1.80

*All data sets were collected at −180°C. AuCN, $K_2Au(CN)_2$; TMLA, trimethyl lead acetate. †Data collected with an R-AXISIIc system (Molecular Structure Corporation). ‡Data collected at the X4A beamline of the National Synchrotron Light Source (NSLS), Brookhaven, NY. §$R_{sym} = 100 \times \Sigma h \Sigma i |I_{hi} - \langle I_h \rangle| / \Sigma h \Sigma i |I_{hi}|$, where *h* are unique reflection indices, I_{hi} are intensities of symmetry-redundant reflections, and $\langle I_h \rangle$ is the mean intensity. ‖Phasing power is the rms value of F_h divided by the rms lack-of-closure error.

REFERENCES AND NOTES

1. G. Sawers, *Antonie Leeuwenhoek* **66**, 57 (1994).
2. M. J. Axley, D. A. Grahame, T. C. Stadtman, *J. Biol. Chem.* **265**, 18213 (1990).
3. M. J. Axley and D. A. Grahame, *ibid.* **266**, 13731 (1991).
4. V. N. Gladyshev, S. V. Khangulov, M. J. Axley, T. C. Stadtman, *Proc. Natl. Acad. Sci. U.S.A.* **91**, 7708 (1994).
5. M. J. Romão *et al.*, *Science* **270**, 1170 (1995).
6. M. K. Chan, S. Mukund, A. Kletzin, M. W. W. Adams, D. C. Rees, *ibid.* **267**, 1463 (1995).
7. H. Schindelin, C. Kisker, J. Hilton, K. V. Rajagopalan, D. C. Rees, *ibid.* **272**, 1615 (1996). The overall fold of *Rhodobacter sphaeroides* DMSO reductase is similar to that of FDH_H.
8. R. Huber *et al.*, *Proc. Natl. Acad. Sci. U.S.A.* **93**, 8846 (1996).
9. T. C. Stadtman, *Annu. Rev. Biochem.* **65**, 83 (1996); R. S. Pilato and E. I. Stiefel, in *Bioinorganic Catalysis*, J. Reedijk, Ed. (Dekker, New York, 1993), chap. 6.
10. A. M. Lesk, *Curr. Opin. Struct. Biol.* **5**, 775 (1995); G. E. Schulz, *ibid.* **2**, 61 (1992).
11. Sequences were obtained from the SWISS-PROT protein sequence data bank [A. Bairoch and B. Boeckmann, *Nucleic Acids Res.* **20**, 2019 (1992)] (accession numbers p07658, p06131, 032176, p24183, and

p46448) and the Protein Identification Resource (PIR) [K. E. Sidman, D. G. George, W. C. Barker, L. T. Hunt, *ibid.* **16**, 1869 (1988)] (accession number s18213).
12. The Mo-ligand distances in the reduced form of FDH_H are as follows: $MGD^{801}S12$, 2.1 Å; $MGD^{801}S13$, 2.3 Å; $MGD^{802}S12$, 2.5 Å; $MGD^{802}S13$, 2.3 Å; and Se, 2.5 Å. In the oxidized form of FDH_H, the Mo-ligand distances are as follows: $MGD^{801}S12$, 2.6 Å; $MGD^{801}S13$, 2.3 Å; $MGD^{802}S12$, 2.4 Å; $MGD^{802}S13$, 2.4 Å; Se, 2.7 Å; and OH, 2.2 Å.
13. M. J. Axley, A. Böck, T. C. Stadtman, *Proc. Natl. Acad. Sci. U.S.A.* **88**, 8450 (1991).
14. EPR spectroscopy provided evidence that the formate-derived proton is located in the vicinity of the Mo(V) center and is slowly exchangeable with water; the proton-accepting group is weakly involved in the electronic ground state of the Mo(V) center and is not a direct ligand to Mo (S. V. Khangulov, V. N. Gladyshev, T. C. Stadtman, in preparation).
15. NMR studies of a $SeCys^{221}$ derivative of subtilisin suggest the presence of a hydrogen bond between the protonated Nε2 of His^{64} and the selenium of $SeCys^{221}$ [K. L. House, A. R. Garber, R. B. Dunlap, J. D. Odom, D. Hilvert, *Biochemistry* **32**, 3468 (1993)].
16. S. K. Das, D. Biswas, R. Maiti, S. Sarkar, *J. Am. Chem. Soc.* **118**, 1387 (1996).
17. G. N. George, J. Hilton, K. V. Rajagopalan, *ibid.*, p. 1113.
18. M. J. Barber, H. L. May, J. G. Ferry, *Biochemistry* **25**, 8150 (1986).
19. J. Dong *et al.*, in preparation.
20. V. N. Gladyshev *et al.*, *J. Biol. Chem.* **271**, 8095 (1996). The results of EPR studies of reduced and oxidized FDH_H crystals are consistent with the presence of a [Mo(IV), $Fe_4S_{4(red)}$] state and a [Mo(VI), $Fe_4S_{4(ox)}$] state, respectively.
21. Z. Otwinowski, in *Proceedings of the CCP4 Study Weekend: Data Collection and Processing*, L. Sawyer, N. Isaacs, S. Bailey, Eds. (SERC Daresbury Laboratory, Warrington, UK, 1993), pp. 56–62.
22. *R-AxisIIc Data Processing Software Version 2.1 Instruction Manual* (Rigaku Corp., 1994).
23. *CCP4: A Suite of Programs for Protein Crystallography* (SERC Collaborative Computing Project No. 4, Daresbury Laboratory, Warrington, UK, 1979).
24. T. A. Jones, J.-Y. Zou, S. W. Cowan, M. Kjelgaard, *Acta Crystallogr. A* **47**, 110 (1991).
25. A. T. Brünger, *X-PLOR Version 3.1, a System for X-ray Crystallography and NMR* (Yale Univ. Press, New Haven, CT, 1992).
26. K. Kraulis, *J. Appl. Crystallogr.* **24**, 946 (1991); D. J. Bacon and W. F. Anderson, *J. Mol. Graphics* **6**, 219 (1988); E. A. Merritt and M. E. P. Murphy, *Acta Crystallogr.* **D50**, 869 (1994).
27. S. V. Evans, *J. Mol. Graphics* **11**, 134 (1993).
28. We thank D. A. Grahame for use of the anaerobic glove chamber and helpful discussions, C. Ogata and staff at HHMI beamline X4A, and Y. Zhang and L. Hannick for help in the synchrotron data collection.

2 August 1996; accepted 14 January 1997

Formation of Actin Stress Fibers and Focal Adhesions Enhanced by Rho-Kinase

Mutsuki Amano, Kazuyasu Chihara, Kazushi Kimura, Yuko Fukata, Nao Nakamura, Yoshiharu Matsuura, Kozo Kaibuchi*

The small guanosine triphosphatase (GTPase) Rho is implicated in the formation of stress fibers and focal adhesions in fibroblasts stimulated by extracellular signals such as lysophosphatidic acid (LPA). Rho-kinase is activated by Rho and may mediate some biological effects of Rho. Microinjection of the catalytic domain of Rho-kinase into serum-starved Swiss 3T3 cells induced the formation of stress fibers and focal adhesions, whereas microinjection of the inactive catalytic domain, the Rho-binding domain, or the pleckstrin-homology domain inhibited the LPA-induced formation of stress fibers and focal adhesions. Thus, Rho-kinase appears to mediate signals from Rho and to induce the formation of stress fibers and focal adhesions.

The small GTPase Rho is inactive in its guanosine diphosphate (GDP)–bound form and active in its guanosine triphosphate (GTP)–bound form (*1*). When cells are stimulated with certain extracellular signals such as LPA, GDP·Rho is believed to be converted to GTP·Rho, which binds to specific targets that mediate its biological functions. Rho participates in signaling pathways that lead to the formation of actin stress fibers and focal adhesions (*2*). Actin stress fibers are linked to integrins at the inner surface of the plasma membrane through focal adhesions (*1*, *2*). Rho also participates in the regulation of cell morphology (*3*), cell aggregation (*4*), cell motility (*5*), cytokinesis (*6*), and smooth muscle contraction (*7*). In budding yeast, RHO1 (a homolog of RhoA) is implicated in the regulation of cell morphology and budding (*8*). Target proteins, the functions of which are modulated by Rho, include protein kinase N (PKN) (*9*), Rho-kinase (*10*) [also called Rho-binding kinase (*11*)], and the myosin-binding subunit (MBS) of myosin phosphatase (*12*). Rho-kinase phosphorylates MBS and consequently inactivates myosin phosphatase (*12*). Rho-kinase phosphorylates myosin light chain and thereby activates myosin adenosine triphosphatase (ATPase) (*13*). Other targets of Rho with unknown functions include rhophilin, p160 Rho-associated coiled-coil–containing protein kinase (ROCK), rhotekin, citron (*9*, *14*), and phosphatidylinositol-4-phosphate 5-kinase (PIP5-K) (*15*). To elucidate the functions of Rho-kinase among these targets of Rho, we produced dominant active and negative forms of Rho-kinase.

Serine-threonine kinases such as protein kinase C (PKC) and Raf are usually composed of regulatory and catalytic domains (*16*). Deletion of the regulatory domains makes PKC and Raf constitutively active, and the regulatory fragments serve as dominant negative forms of the kinases (*17*, *18*). Rho-kinase is composed of catalytic, coiled-coil, Rho-binding, and pleckstrin-homology domains. We

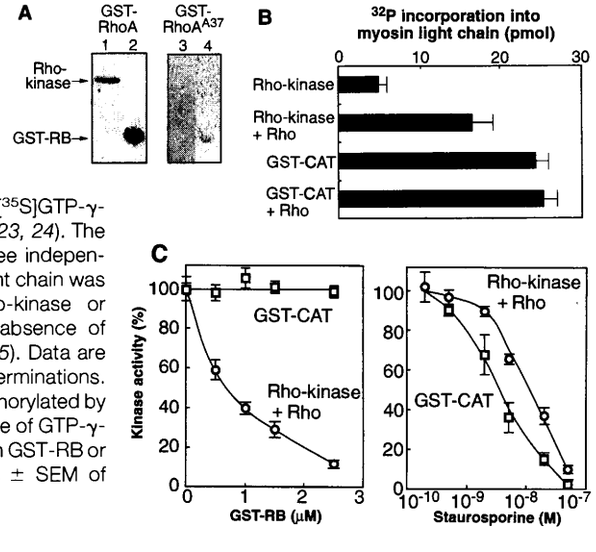

Fig. 1. Dominant active and negative forms of Rho-kinase. (**A**) Nitrocellulose membranes containing the purified native Rho-kinase (lanes 1 and 3) and GST-RB (lanes 2 and 4) separated by SDS-PAGE were probed with [^{35}S]GTP-γ-S·GST-RhoA (lanes 1 and 2) or [^{35}S]GTP-γ-S·GST-RhoA^{A37} (lanes 3 and 4) (*23*, *24*). The results are representative of three independent experiments. (**B**) Myosin light chain was phosphorylated by native Rho-kinase or GST-CAT in the presence or absence of GTP-γ-S·GST-RhoA (1.5 μM) (*25*). Data are means ± SEM of triplicate determinations. (**C**) Myosin light chain was phosphorylated by native Rho-kinase in the presence of GTP-γ-S·GST-RhoA or by GST-CAT with GST-RB or staurosporine. Data are means ± SEM of triplicate determinations.

M. Amano, K. Chihara, Y. Fukata, N. Nakamura, K. Kaibuchi, Division of Signal Transduction, Nara Institute of Science and Technology, Ikoma 630-01, Japan.
K. Kimura, Division of Signal Transduction, Nara Institute of Science and Technology, Ikoma 630-01, Japan, and Second Department of Anatomy, Kyoto University Faculty of Medicine, Kyoto 606, Japan.
Y. Matsuura, Department of Virology II, National Institute of Health, Tokyo 162, Japan.
*To whom correspondence should be addressed.